Gain-Loss-Induced Hybrid Skin-Topological Effect

Yaohua Li,[1] Chao Liang,[1] Chenyang Wang,[1] Cuicui Lu,[2,3] and Yong-Chun Liu[1,4,*]
[1]State Key Laboratory of Low-Dimensional Quantum Physics, Department of Physics, Tsinghua University, Beijing 100084, People's Republic of China
[2]Key Laboratory of Advanced Optoelectronic Quantum Architecture and Measurements of Ministry of Education, Beijing Key Laboratory of Nanophotonics and Ultrafine Optoelectronic Systems, School of Physics, Beijing Institute of Technology, Beijing 100081, China
[3]Collaborative Innovation Center of Light Manipulations and Applications, Shandong Normal University, Jinan 250358, China
[4]Frontier Science Center for Quantum Information, Beijing 100084, People's Republic of China

(Received 27 January 2022; accepted 13 May 2022; published 1 June 2022)

Non-Hermitian topological effects are of crucial importance both in fundamental physics and applications. Here we discover the gain-loss-induced hybrid second-order skin-topological effect and the $\mathcal{PT}$ phase transition in skin-topological modes. By studying a non-Hermitian Haldane model, we find that the topological edge modes are localized on a special type of corner, while the bulk modes remain extended. Such an effect originates from the interplay between gain, loss, and the chiral edge currents induced by the nonlocal flux, which can be characterized by considering the properties of the edge sites as a one-dimensional chain. We establish a relation between the skin-topological effect and the $\mathcal{PT}$ symmetries belonging to different edges. Moreover, we discover the $\mathcal{PT}$ phase transition with the emergence of exceptional points between pairs of skin-topological modes. Our results pave the way for the investigation of non-Hermitian topological physics and $\mathcal{PT}$ phase transition in higher-dimensional systems.

DOI: 10.1103/PhysRevLett.128.223903

Introduction.—Non-Hermitian Hamiltonians emerge as a simple but effective method to describe most real physical systems which are open in the environment [1]. In general, non-Hermitian Hamiltonians possesses complex eigenvalues and biorthogonal eigenmodes, which are distinctly different from the properties of Hermitian Hamiltonians. Exceptional points (EPs) appear when two or more eigenmodes coalesce, which also leads to the parity-time ($\mathcal{PT}$) phase transition in a system with $\mathcal{PT}$ symmetry [2–9]. Recently there are growing efforts, both theoretically [10–15] and experimentally [16–21], to study the basic topology and dynamics under the non-Hermitian Hamiltonians. A most intriguing example is the non-Hermitian skin effect, where the non-Hermicity drives the system eigenmodes to approach the boundary, with the breakdown of the Hermitian bulk-boundary correspondence [22–29].

The nontrivial interplay between the non-Hermitian skin effect and the topological effect has led to the concept of hybrid skin-topological effect, where the skin effect acts only on the topological edge modes but not the bulk modes [30–32], showing both the properties of non-Hermitian localization and topological localization. It represents a kind of higher-order skin effect [33–35], which exhibits higher-dimensional (more than one dimension) robustness, without the requirement of higher-order topological phenomena. There are two kinds of non-Hermitian Hamiltonians, describing nonreciprocal systems with asymmetric coupling strengths [36–43] and gain-loss systems [44–54]. Except for some special cases in one-dimensional (1D) systems [36,46,55], they are inequivalent due to different origins of non-Hermicity, especially in higher-dimensional systems. At present, the higher-order skin effects have only been studied in systems with asymmetric coupling strengths [33–35], while the exploration of higher-order skin effect in gain-loss systems remains a challenge. Compared with asymmetric coupling strengths, there are more mature technologies to generate gain and loss in various systems. Moreover, the introduction of $\mathcal{PT}$ symmetry will greatly enrich the physics in higher-dimensional systems.

Here we find that hybrid second-order skin-topological effect can be induced by on-site gain and loss, by analyzing a non-Hermitian Haldane model. The discovered skin-topological modes are localized on a special type of corner, with exponential distributions along the edges, showing both the characteristics of non-Hermitian skin modes and topological edge modes. Such an effect originates from the interplay between gain, loss, and the chiral edge currents induced by the nonlocal flux, which are distinctly different

from the conventional skin-topological modes where asymmetric coupling strengths are indispensable. We find that the skin-topological effect can be intuitively obtained by only considering the properties of the edge sites as a 1D chain. At the same time, we show that the skin-topological effect can be predicted by analyzing the $\mathcal{PT}$ symmetries belonging to different edges, e.g., zigzag and armchair edges. Moreover, we discover the $\mathcal{PT}$ phase transition with the emergence of exceptional points between pairs of skin-topological modes. Beyond the EPs, the $\mathcal{PT}$ symmetry is spontaneously broken and the skin-topological modes have different distributions along gain and loss edges. Besides the Chern insulator phase where we obtain skin-topological modes, the calculation of the Chern number reveals a phase diagram with rich phases and non-Hermitian topologies.

Model.—The Haldane model is a crucial model to describe topological insulators [56,57]. Here we consider a non-Hermitian Haldane model on the honeycomb lattice with complex on-site mass terms $\pm(m+i\gamma)$ for the two sites in each subcell, as shown in Fig. 1(a). The imaginary parts $\pm\gamma$ correspond to the on-site gain and loss, which play the key role in this Letter. The nearest-neighbor couplings are $t_1 = 1$, and the next-nearest-neighbor couplings are $t_2 e^{i\phi}$ with amplitude t_2 and phase ϕ. In the periodic boundary condition (PBC) along both x and y directions, the k-space Hamiltonian is given by $H_k = h_0 I + h_1\sigma_x + h_2\sigma_y + (h_3 + i\gamma)\sigma_z$, where I is the identity matrix, $\sigma_{x,y,z}$ are Pauli matrices, and

$$
\begin{aligned}
h_0 &= 2t_2\cos\phi \sum_{j=1,2,3} \sin(\mathbf{k}\cdot\mathbf{c}_j),\\
h_1 &= t_1[1+\cos(\mathbf{k}\cdot\mathbf{c}_2)+\cos(\mathbf{k}\cdot\mathbf{c}_3)],\\
h_2 &= t_1[\sin(\mathbf{k}\cdot\mathbf{c}_2)-\sin(\mathbf{k}\cdot\mathbf{c}_3)],\\
h_3 &= m - 2t_2\sin\phi \sum_{j=1,2,3} \sin(\mathbf{k}\cdot\mathbf{c}_j).
\end{aligned}
\tag{1}
$$

Here $\mathbf{k} = (k_x, k_y)$ is the wave vector, and the lattice vectors are $\mathbf{c}_1 = (\sqrt{3}, 0)$, $\mathbf{c}_2 = (-\sqrt{3}/2, -3/2)$, and $\mathbf{c}_3 = (-\sqrt{3}/2, 3/2)$. In the Hermitian case, topological phase transition occurs at $m = \pm 3\sqrt{3}t_2\sin\phi$ between phases characterized by different Chern numbers. The nonzero Chern number ensures the existence of chiral topological edge modes in the open boundary condition (OBC) [56].

Skin-topological modes.—In the non-Hermitian case, we find that the topological edge modes have exponential distributions localized in the corners, as shown in Figs. 1(b)–1(f). For the system with size $L \times L$, all the edge modes with the number scaling as $\mathcal{O}(L)$ are localized into the corners continuously without the change of the intrinsic topology. Note that these modes are neither second-order topological modes [scaling as $\mathcal{O}(1)$], nor first-order skin modes [scaling as $\mathcal{O}(L^2)$]. Instead, these are hybrid skin-topological modes, which possess the properties of both skin modes and topological modes.

It is clearer when we take the zigzag edges separately as a 1D chain. As shown in Fig. 1(b), there is nonlocal flux ϕ over each triangular plaquette. This leads to the existence of chiral edge currents, i.e., excitations on different sublattices move in different directions [58]. When we include the on site gain and loss in the sublattices, the eigenmodes of the 1D chain are all localized to one side, leading to the 1D skin effect, as shown in Fig. 1(c). The localized direction is along (opposite to) the edge current of the gain (loss) modes. The asymmetric currents indicate another kind of nonreciprocal coupling, which come from the complex next-nearest-neighbor couplings, i.e., the nonzero coupling phases. When we consider the 2D honeycomb lattice, the nonreciprocity cancels out in the bulk as there are only local flux with no asymmetric currents. The gain and loss are also balanced in the bulk, so the first-order skin effect disappears in the bulk. However, the net reciprocity is spontaneously broken at the zigzag edges with nonlocal flux, leading to the second-order skin effect. As compared in Figs. 1(d)–1(f), the skin effect of the edge modes appears when $\gamma \neq 0$, and the localized directions agree well with the

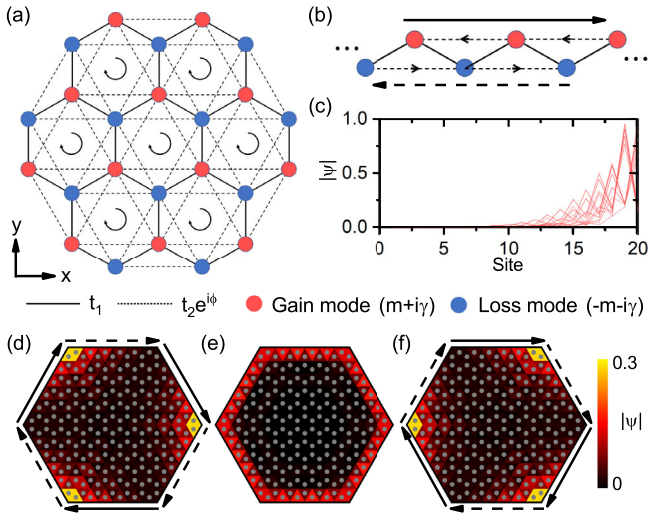

FIG. 1. Hybrid skin-topological modes in non-Hermitian Haldane model. (a) Schematic of the non-Hermitian lattice. The red (blue) circles denote sites with opposite on-site mass terms $\pm(m+i\gamma)$. (b) Zigzag edge of the honeycomb lattice as a 1D chain, which has non-Hermitian skin effect with on-site gain and loss. The long solid (dashed) arrow indicates the chiral edge current along (opposite to) the localized direction [similar in (d) and (f)]. The black arrows in (a) and middle-line arrows in (b) indicate the directions of the next-nearest-neighbor couplings $t_2 e^{i\phi}$. (c) Profile of all eigenmodes for the 1D chain in (b) with 20 sites. The on-site gain and loss are $\gamma = 3$. (d)–(f) The chiral edge mode for $\gamma = 0$ (e) become skin-topological modes for $\gamma = -0.6$ (d) and $\gamma = 0.6$ (f) with different localized directions. Every triangle with a gray circle denotes a site. Here the chiral edge mode propagates clockwise. Other parameters are $t_2 = 0.2$ and $\phi = \pi/2$.

law we obtained from the 1D results. There are two types of corners with localized directions at both sides toward or away from the corner. The distributions of the skin-topological modes are mainly at the first one.

Such a skin-topological effect depends on the type of the edges, as the net flux varies for different edges. Both zigzag and bearded edges support skin-topological modes, while the armchair edges do not due to the canceled flux (see the Supplemental Material [59]).

This effect can also be understood using the projected band structures, which allow us to study the properties of each type of edge separately. As plotted in Figs. 2(a) and 2(e), we consider two perpendicular directions to truncate the lattices and obtain effective 1D models in PBC along the x direction (xPBC/yOBC) with zigzag edges, and xOBC/yPBC with armchair edges. In Figs. 2(b)–2(c) and 2(f)–2(g), we plot the energy spectra in the above two cases. In the first case, the eigenenergies of the edge bands are not real and form a loop [Fig. 2(c)]. According to the result in the 1D model that the bands with loops enclosing a point gap with nonzero winding numbers will exhibit skin effect [27,29], we can find that the skin-topological modes appear in this case, i.e., along the zigzag edges (x direction). In the second case, two edge bands coincide into a line in the real axis [Fig. 2(g)], indicating the absence of skin-topological modes along the armchair edges (y direction).

$\mathcal{PT}$ symmetries.—Because of the diversity of the parity operations, different $\mathcal{PT}$ symmetries can be defined for the above two cases. Letting $\mathcal{P}_1 = \{\delta_{p,2n+1-q}\}$ ($\delta_{p,q}$ is the Kronecker function, p and q are matrix indices) and $\mathcal{P}_2 = \bigoplus_n \sigma_x$ with n being the number of unit cells along the open boundary direction, we obtain

$$\mathcal{P}_1\mathcal{T}H_{k_x}(\mathcal{P}_1\mathcal{T})^{-1} = H_{k_x},$$
$$\mathcal{P}_2\mathcal{T}H_{k_y}(\mathcal{P}_2\mathcal{T})^{-1} = H'_{k_y}, \tag{2}$$

where $\mathcal{T}$ is the time-reversal operator and H_{k_x} and H_{k_y} (H'_{k_y}) are the Bloch Hamiltonians of the two cases. We note that H_{k_y} and H'_{k_y} are obtained from the Fourier transform with different unit cells but are equivalent in the operator form as they describe the same structure [59]. In the first case, $\mathcal{P}_1\mathcal{T}$ is a global operation which maps any mode localized in one boundary into the other boundary; thus along the open boundary directions (y direction) the skin-topological modes cannot exist. This is verified in Fig. 2(d), which plots the mode profiles of the two edge modes marked in Fig. 2(c). They are localized at opposite boundaries, indicating no skin effect along the y direction. Differently, in the second case $\mathcal{P}_2\mathcal{T}$ is a local operation with mapping inside each subcell, so skin effect is allowed. As shown in Fig. 2(h), the two edge modes marked in Fig. 2(g) are localized at the same boundary, which reveals that skin effect exists along the x direction.

$\mathcal{PT}$ phase transition and exceptional points.—Here we concentrate on the lattice with a hexagonal boundary and zigzag edges, which still possesses $\mathcal{PT}$ symmetry for $m = 0$. The parity operator here becomes a mirror operator,

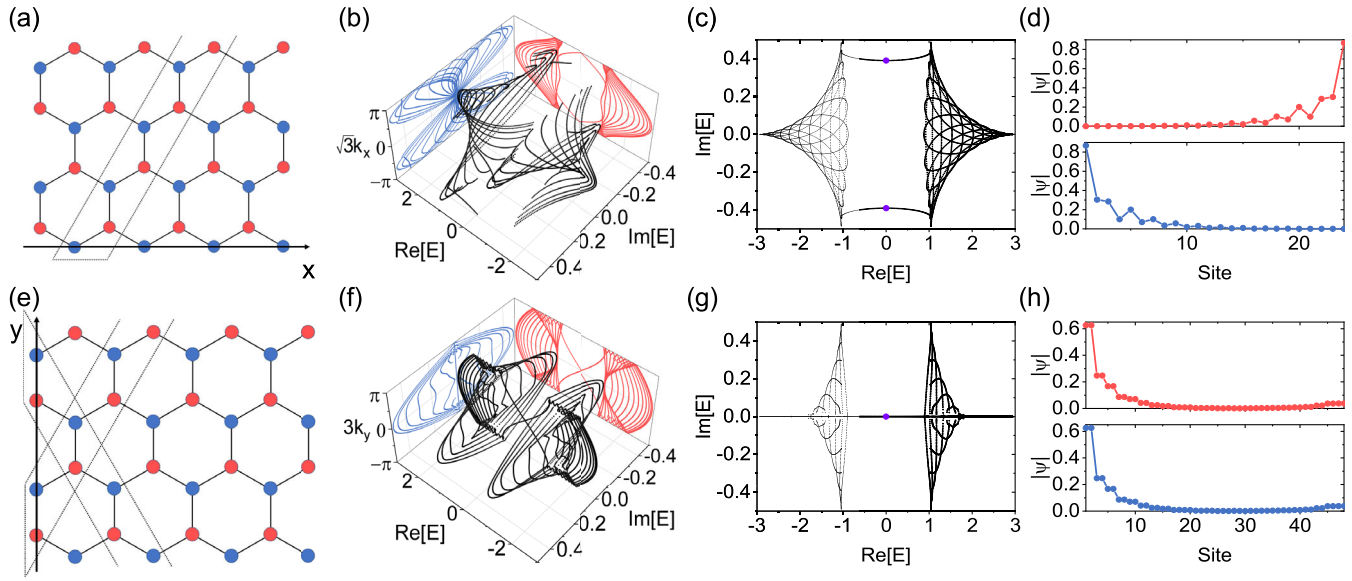

FIG. 2. Projected band structures along different axes and edge modes. (a)–(d) xPBC/yOBC. (e)–(h) xOBC/yPBC. (a),(e) Schematic of the Fourier transform. The dotted parallelograms are choices of unit cells for Fourier transform. (b),(f) Energy spectra (black curves) in $E - k_x$ space (b) and $E - k_y$ space (f). The red and blue curves are 2D projections on the corresponding plane. (c),(g) Projection of the real and imaginary parts of the energy spectra in (b) and (f). (d),(h) Two edge modes with eigenenergies indicated by the purple dots in (c) and (g). The horizontal axes correspond to the site numbers along the open boundary direction. The parameters are $m = 0$, $\gamma = 0.5$, $t_2 = 0.2$, and $\phi = \pi/2$.

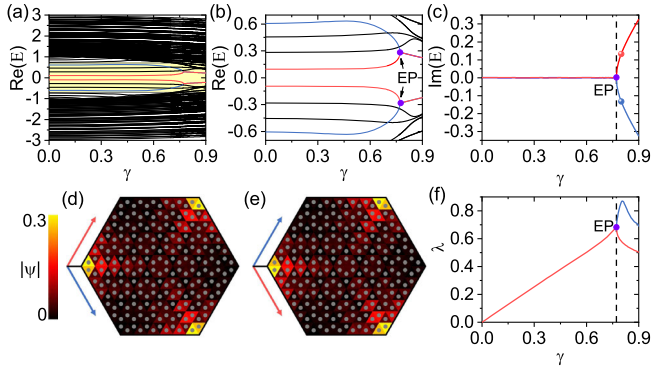

FIG. 3. The energy spectra and EPs of the lattice with hexagonal boundary. (a) The real part of the eigenenergies as a function of the gain-loss parameter γ. The red and blue curves represent four skin-topological modes. (b) Enlarged view of the yellow area in (a). The purple circles indicate the EPs. (c) The imaginary part of the eigenvalues for the four skin-topological modes highlighted in (a) and (b). (d),(e) The distribution of the eigenmodes indicated by blue (d) and red (e) points in (c). (f) The decay coefficients of the eigenmode amplitudes along the edges as functions of γ. The red (blue) curve corresponds to the edge indicated by the red (blue) arrows in (d) and (e). Other parameters are $m = 0$, $t_2 = 0.2$, and $\phi = \pi/2$.

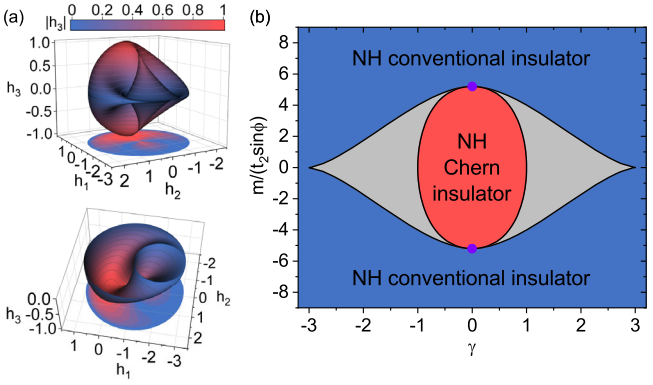

FIG. 4. The topology and phase diagram of the non-Hermitian Haldane model. (a) The surface $\mathbb{S}$ mapped from the first Brillouin zone, i.e., mapping from (k_x, k_y) to (h_1, h_2, h_3). The color map represents the magnitude of h_3. The parameters are $m = 0$, $t_2 = 0.2$, and $\phi = \pi/2$. The density map below is the projection of the surface. The bottom figure is half of the top figure for $h_3 < 0$. (b) The phase diagram. The red area is the non-Hermitian Chern insulator phase where $\mathcal{C} = 1$. The blue area is the non-Hermitian conventional insulator phase where $\mathcal{C} = 0$. The gray area is a gapless phase with EPs between two bulk bands. The black curves are phase boundaries. The purple points indicate the Hermitian phase boundary with the emergence of Dirac points.

and there are three mirror axes across the corners due to the C_3 symmetry. When the gain-loss parameter γ is small, the system will be in the $\mathcal{PT}$-symmetric phase, with symmetric distribution of the skin-topological modes and real eigenenergies. When increasing γ, EPs emerge between pairs of skin-topological modes, with spontaneous breaking of $\mathcal{PT}$ symmetry. For even site numbers along every edge, EPs of edge modes will appear in pairs with nonzero eigenenergies, as shown in Figs. 3(a)–3(c). In the $\mathcal{PT}$-symmetry-broken phase with a large γ, the distributions of the skin-topological modes are $\mathcal{PT}$-asymmetric, as shown in Figs. 3(d)–3(e).

The skin-topological modes have exponential distribution along the edges, so we can define $|\psi_{p,n}| \propto e^{-\lambda n}$, where λ is the decay coefficient and $\psi_{p,n}$ is the amplitude at the nth site in the p-type edges, with $p = G(L)$ representing the edges with gain (loss) modes in the outermost layer. In Fig. 3(f), we plot the decay coefficients along G (red) and L (blue) edges as functions of γ. In the $\mathcal{PT}$-symmetric phase, the decay coefficients along two kinds of edges have the same values and follow a linear scaling with γ. In the $\mathcal{PT}$-symmetry-broken phase, the decay coefficients become different, where the skin-topological modes have more distributions and a smaller decay coefficient along one type of edge.

Phase diagram.—The phase diagram of the gain-loss Haldane model is determined by the Chern number, which can be obtained from the integral of the Berry curvature over the first Brillouin zone [60]. As shown in Fig. 4(a), the first Brillouin zone can be mapped into a surface $\mathbb{S}$ in the 3D space $\mathbb{R}^3$. In the Hermitian case, when the surface $\mathbb{S}$ in the 3D space $\mathbb{R}^3$ encloses the origin $\mathbb{O}$, i.e., the only gap-closing point, the lattice becomes a Chern insulator with nonzero Chern number. However, in the non-Hermitian case, the origin $\mathbb{O}$ is no longer the gap-closing point. On the contrary, the bulk bands are degenerate at a circle $\mathbb{L}$: $(h_1^2 + h_2^2 = \gamma^2,\ h_3 = 0)$, and the system topology depends on whether the surface $\mathbb{S}$ encloses the circle $\mathbb{L}$.

Figure 4(b) presents the phase diagram as functions of the scaled on-site mass $m/(t_2 \sin\phi)$ and the gain-loss parameter γ. There are two gapped phases and one gapless phase. The first gapped phase with $\mathcal{C} = 1$ in red is the non-Hermitian Chern insulator phase. The nonzero Chern number ensures the existence of skin-topological modes in this phase. In the above discussion about the skin-topological effect, we have used $m = 0$, $t_2 = 0.2$, $\phi = \pi/2$, and $|\gamma| < 1$, which are all in this phase. We note that the skin-topological effect exists in all the red area, even for $m \neq 0$ and $\phi \neq \pi/2$, i.e., without the particle-hole symmetry. Another gapped phase with $\mathcal{C} = 0$ in blue is the non-Hermitian conventional insulator phase, which is trivial with no topological or skin modes.

When the circle $\mathbb{L}$ intersects with the surface $\mathbb{S}$, EPs emerge between two bulk bands at the intersections. In this way, we obtain the gray area where the bulk bands are gapless with EPs. It has two phase boundaries indicated by the solid curves in Fig. 4(b). The inside boundary with small $|\gamma|$ corresponds to the case that $\mathbb{S}$ encloses $\mathbb{L}$ except for the intersections, while the outside boundary corresponds to the contrary case. These two phase boundaries

coincide when $\gamma = 0$, where the six EPs become six Dirac points [59].

Conclusion.—In summary, we discover the gain-loss-induced hybrid skin-topological effect, where on-site gain and loss are used to obtain the hybrid second-order skin-topological modes. By investigating the non-Hermitian Haldane model, we find that the topological edge modes are localized on a special type of corner, while the bulk modes remain extended, showing that the skin effect only acts on the topological edge modes but not the bulk modes. Such an effect originates from the interplay between gain, loss, and the chiral edge currents induced by the nonlocal flux, and it can be intuitively obtained by only considering the properties of the edge sites as a 1D chain. We establish a relation between the skin-topological effect and the $\mathcal{PT}$ symmetries belonging to different edges. For example, the $\mathcal{P}_2\mathcal{T}$ symmetry of the zigzag edges allows for the existence of skin-topological modes, while the $\mathcal{P}_1\mathcal{T}$ symmetry of the armchair edges does not. We also discover the $\mathcal{PT}$ phase transition with the emergence of EPs between pairs of skin-topological modes. Furthermore, we obtain a rich phase diagram in the non-Hermitian situation, and find that the Chern number reveals non-Hermitian topology in the 3D space $\mathbb{R}^3$ between the Hamiltonian surface $\mathbb{S}$ and the exceptional circle $\mathbb{L}$. Our Letter offers the opportunity for manipulating non-Hermitian and topological properties through gain-loss control, and sheds light on studying $\mathcal{PT}$ phase transition in higher-dimensional systems.

We thank Prof. C. T. Chan at the Hong Kong University of Science and Technology for helpful discussions. This work is supported by the Key-Area Research and Development Program of Guangdong Province (Grant No. 2019B030330001), the National Natural Science Foundation of China (NSFC) (Grants No. 92050110, No. 91736106, No. 11674390, No. 91836302, No. 91850117, and No. 11654003), and the National Key R&D Program of China (Grant No. 2018YFA0306504).

Note added.—During the peer review process, we noticed a related work appear; see Ref. [61].

*ycliu@tsinghua.edu.cn

[1] Y. Ashida, Z. Gong, and M. Ueda, Non-Hermitian physics, Adv. Phys. **69**, 249 (2020).

[2] C. M. Bender and S. Boettcher, Real Spectra in Non-Hermitian Hamiltonians Having $\mathcal{PT}$ Symmetry, Phys. Rev. Lett. **80**, 5243 (1998).

[3] A. Guo, G. J. Salamo, D. Duchesne, R. Morandotti, M. Volatier-Ravat, V. Aimez, G. A. Siviloglou, and D. N. Christodoulides, Observation of $\mathcal{PT}$-Symmetry Breaking in Complex Optical Potentials, Phys. Rev. Lett. **103**, 093902 (2009).

[4] A. Regensburger, C. Bersch, M.-A. Miri, G. Onishchukov, D. N. Christodoulides, and U. Peschel, Parity-time synthetic photonic lattices, Nature (London) **488**, 167 (2012).

[5] S. Weimann, M. Kremer, Y. Plotnik, Y. Lumer, S. Nolte, K. G. Makris, M. Segev, M. C. Rechtsman, and A. Szameit, Topologically protected bound states in photonic parity-time-symmetric crystals, Nat. Mater. **16**, 433 (2017).

[6] R. El-Ganainy, K. G. Makris, M. Khajavikhan, Z. H. Musslimani, S. Rotter, and D. N. Christodoulides, Non-Hermitian physics and PT symmetry, Nat. Phys. **14**, 11 (2018).

[7] X. Ni, D. Smirnova, A. Poddubny, D. Leykam, Y. Chong, and A. B. Khanikaev, $\mathcal{PT}$ phase transitions of edge states at $\mathcal{PT}$ symmetric interfaces in non-Hermitian topological insulators, Phys. Rev. B **98**, 165129 (2018).

[8] M. Kremer, T. Biesenthal, L. J. Maczewsky, M. Heinrich, R. Thomale, and A. Szameit, Demonstration of a two-dimensional $\mathcal{PT}$-symmetric crystal, Nat. Commun. **10**, 435 (2019).

[9] S. Xia, D. Kaltsas, D. Song, I. Komis, J. Xu, A. Szameit, H. Buljan, K. G. Makris, and Z. Chen, Nonlinear tuning of PT symmetry and non-Hermitian topological states, Science **372**, 72 (2021).

[10] S. Yao, F. Song, and Z. Wang, Non-Hermitian Chern Bands, Phys. Rev. Lett. **121**, 136802 (2018).

[11] K. Kawabata, K. Shiozaki, M. Ueda, and M. Sato, Symmetry and Topology in Non-Hermitian Physics, Phys. Rev. X **9**, 041015 (2019).

[12] T. Liu, Y.-R. Zhang, Q. Ai, Z. Gong, K. Kawabata, M. Ueda, and F. Nori, Second-Order Topological Phases in Non-Hermitian Systems, Phys. Rev. Lett. **122**, 076801 (2019).

[13] X.-W. Luo and C. Zhang, Higher-Order Topological Corner States Induced by Gain and Loss, Phys. Rev. Lett. **123**, 073601 (2019).

[14] Z. Zhang, M. Rosendo López, Y. Cheng, X. Liu, and J. Christensen, Non-Hermitian Sonic Second-Order Topological Insulator, Phys. Rev. Lett. **122**, 195501 (2019).

[15] H. Wu, B.-Q. Wang, and J.-H. An, Floquet second-order topological insulators in non-Hermitian systems, Phys. Rev. B **103**, L041115 (2021).

[16] W. Song, W. Sun, C. Chen, Q. Song, S. Xiao, S. Zhu, and T. Li, Breakup and Recovery of Topological Zero Modes in Finite Non-Hermitian Optical Lattices, Phys. Rev. Lett. **123**, 165701 (2019).

[17] H. Zhao, X. Qiao, T. Wu, B. Midya, S. Longhi, and L. Feng, Non-Hermitian topological light steering, Science **365**, 1163 (2019).

[18] S. Weidemann, M. Kremer, T. Helbig, T. Hofmann, A. Stegmaier, M. Greiter, R. Thomale, and A. Szameit, Topological funneling of light, Science **368**, 311 (2020).

[19] B. Hu, Z. Zhang, H. Zhang, L. Zheng, W. Xiong, Z. Yue, X. Wang, J. Xu, Y. Cheng, X. Liu, and J. Christensen, Non-Hermitian topological whispering gallery, Nature (London) **597**, 655 (2021).

[20] F. E. Öztürk, T. Lappe, G. Hellmann, J. Schmitt, J. Klaers, F. Vewinger, J. Kroha, and M. Weitz, Observation of a non-Hermitian phase transition in an optical quantum gas, Science **372**, 88 (2021).

[21] K. Wang, A. Dutt, K. Y. Yang, C. C. Wojcik, J. Vučković, and S. Fan, Generating arbitrary topological windings of a non-Hermitian band, Science **371**, 1240 (2021).
[22] F. K. Kunst, E. Edvardsson, J. C. Budich, and E. J. Bergholtz, Biorthogonal Bulk-Boundary Correspondence in Non-Hermitian Systems, Phys. Rev. Lett. **121**, 026808 (2018).
[23] K. Yokomizo and S. Murakami, Non-Bloch Band Theory of Non-Hermitian Systems, Phys. Rev. Lett. **123**, 066404 (2019).
[24] F. Song, S. Yao, and Z. Wang, Non-Hermitian Topological Invariants in Real Space, Phys. Rev. Lett. **123**, 246801 (2019).
[25] E. Edvardsson, F. K. Kunst, and E. J. Bergholtz, Non-Hermitian extensions of higher-order topological phases and their biorthogonal bulk-boundary correspondence, Phys. Rev. B **99**, 081302(R) (2019).
[26] T. Helbig, T. Hofmann, S. Imhof, M. Abdelghany, T. Kiessling, L. W. Molenkamp, C. H. Lee, A. Szameit, M. Greiter, and R. Thomale, Generalized bulk-boundary correspondence in non-Hermitian topolectrical circuits, Nat. Phys. **16**, 747 (2020).
[27] N. Okuma, K. Kawabata, K. Shiozaki, and M. Sato, Topological Origin of Non-Hermitian Skin Effects, Phys. Rev. Lett. **124**, 086801 (2020).
[28] Z. Yang, K. Zhang, C. Fang, and J. Hu, Non-Hermitian Bulk-Boundary Correspondence and Auxiliary Generalized Brillouin Zone Theory, Phys. Rev. Lett. **125**, 226402 (2020).
[29] K. Zhang, Z. Yang, and C. Fang, Correspondence between Winding Numbers and Skin Modes in Non-Hermitian Systems, Phys. Rev. Lett. **125**, 126402 (2020).
[30] X. Zhang, Y. Tian, J.-H. Jiang, M.-H. Lu, and Y.-F. Chen, Observation of higher-order non-Hermitian skin effect, Nat. Commun. **12**, 5377 (2021).
[31] C. H. Lee, L. Li, and J. Gong, Hybrid Higher-Order Skin-Topological Modes in Nonreciprocal Systems, Phys. Rev. Lett. **123**, 016805 (2019).
[32] D. Zou, T. Chen, W. He, J. Bao, C. H. Lee, H. Sun, and X. Zhang, Observation of hybrid higher-order skin-topological effect in non-Hermitian topolectrical circuits, Nat. Commun. **12**, 7201 (2021).
[33] K. Kawabata, M. Sato, and K. Shiozaki, Higher-order non-Hermitian skin effect, Phys. Rev. B **102**, 205118 (2020).
[34] R. Okugawa, R. Takahashi, and K. Yokomizo, Second-order topological non-Hermitian skin effects, Phys. Rev. B **102**, 241202(R) (2020).
[35] Y. Fu, J. Hu, and S. Wan, Non-Hermitian second-order skin and topological modes, Phys. Rev. B **103**, 045420 (2021).
[36] S. Yao and Z. Wang, Edge States and Topological Invariants of Non-Hermitian Systems, Phys. Rev. Lett. **121**, 086803 (2018).
[37] K. Kawabata, K. Shiozaki, and M. Ueda, Anomalous helical edge states in a non-Hermitian Chern insulator, Phys. Rev. B **98**, 165148 (2018).
[38] C. Yin, H. Jiang, L. Li, R. Lü, and S. Chen, Geometrical meaning of winding number and its characterization of topological phases in one-dimensional chiral non-Hermitian systems, Phys. Rev. A **97**, 052115 (2018).
[39] T. Hofmann, T. Helbig, C. H. Lee, M. Greiter, and R. Thomale, Chiral Voltage Propagation and Calibration in a Topolectrical Chern Circuit, Phys. Rev. Lett. **122**, 247702 (2019).
[40] C. H. Lee and R. Thomale, Anatomy of skin modes and topology in non-Hermitian systems, Phys. Rev. B **99**, 201103(R) (2019).
[41] L. Li, C. H. Lee, and J. Gong, Topological Switch for Non-Hermitian Skin Effect in Cold-Atom Systems with Loss, Phys. Rev. Lett. **124**, 250402 (2020).
[42] C. Liang, B. Liu, A.-N. Xu, X. Wen, C. Lu, K. Xia, M. K. Tey, Y.-C. Liu, and L. You, Collision-Induced Broadband Optical Nonreciprocity, Phys. Rev. Lett. **125**, 123901 (2020).
[43] X. Huang, C. Lu, C. Liang, H. Tao, and Y.-C. Liu, Loss-induced nonreciprocity, Light Sci. Appl. **10**, 30 (2021).
[44] B. Peng, Ş. K. Özdemir, S. Rotter, H. Yilmaz, M. Liertzer, F. Monifi, C. M. Bender, F. Nori, and L. Yang, Loss-induced suppression and revival of lasing, Science **346**, 328 (2014).
[45] X.-W. Xu, Y.-x. Liu, C.-P. Sun, and Y. Li, Mechanical $\mathcal{PT}$ symmetry in coupled optomechanical systems, Phys. Rev. A **92**, 013852 (2015).
[46] T. E. Lee, Anomalous Edge State in a Non-Hermitian Lattice, Phys. Rev. Lett. **116**, 133903 (2016).
[47] Y.-L. Liu, R. Wu, J. Zhang, Ş. K. Özdemir, L. Yang, F. Nori, and Y.-x. Liu, Controllable optical response by modifying the gain and loss of a mechanical resonator and cavity mode in an optomechanical system, Phys. Rev. A **95**, 013843 (2017).
[48] G. Harari, M. A. Bandres, Y. Lumer, M. C. Rechtsman, Y. D. Chong, M. Khajavikhan, D. N. Christodoulides, and M. Segev, Topological insulator laser: Theory, Science **359**, eaar4003 (2018).
[49] F. Song, S. Yao, and Z. Wang, Non-Hermitian Skin Effect and Chiral Damping in Open Quantum Systems, Phys. Rev. Lett. **123**, 170401 (2019).
[50] J. Li, A. K. Harter, J. Liu, L. de Melo, Y. N. Joglekar, and L. Luo, Observation of parity-time symmetry breaking transitions in a dissipative Floquet system of ultracold atoms, Nat. Commun. **10**, 855 (2019).
[51] P. Gao, M. Willatzen, and J. Christensen, Anomalous Topological Edge States in Non-Hermitian Piezophononic Media, Phys. Rev. Lett. **125**, 206402 (2020).
[52] P. Reséndiz-Vázquez, K. Tschernig, A. Perez-Leija, K. Busch, and R. J. León-Montiel, Topological protection in non-Hermitian Haldane honeycomb lattices, Phys. Rev. Research **2**, 013387 (2020).
[53] H. Xue, Q. Wang, B. Zhang, and Y. D. Chong, Non-Hermitian Dirac Cones, Phys. Rev. Lett. **124**, 236403 (2020).
[54] Y. Yi and Z. Yang, Non-Hermitian Skin Modes Induced by On-Site Dissipations and Chiral Tunneling Effect, Phys. Rev. Lett. **125**, 186802 (2020).
[55] E. J. Bergholtz, J. C. Budich, and F. K. Kunst, Exceptional topology of non-Hermitian systems, Rev. Mod. Phys. **93**, 015005 (2021).
[56] F. D. M. Haldane, Model for a Quantum Hall Effect without Landau Levels: Condensed-Matter Realization of the "Parity Anomaly", Phys. Rev. Lett. **61**, 2015 (1988).

[57] G. Jotzu, M. Messer, R. Desbuquois, M. Lebrat, T. Uehlinger, D. Greif, and T. Esslinger, Experimental realization of the topological Haldane model with ultracold fermions, Nature (London) **515**, 237 (2014).

[58] H. Cai, J. Liu, J. Wu, Y. He, S.-Y. Zhu, J.-X. Zhang, and D.-W. Wang, Experimental Observation of Momentum-Space Chiral Edge Currents in Room-Temperature Atoms, Phys. Rev. Lett. **122**, 023601 (2019).

[59] See Supplemental Material http://link.aps.org/supplemental/10.1103/PhysRevLett.128.223903 for more details.

[60] The Chern number can be calculated as $\mathcal{C} = \frac{1}{2\pi}\int_{\mathrm{BZ}} d^2k\mathbf{\Omega}(\mathbf{k})$, where $\mathbf{\Omega}(\mathbf{k}) = -\frac{1}{2}(\partial_{k_x}\mathbf{h} \times \partial_{k_y}\mathbf{h}) \cdot \mathbf{h}$ is the Berry curvature and BZ is the first Brillouin zone.

[61] W. Zhu and J. Gong, Hybrid skin-topological modes without asymmetric couplings, arXiv:2203.03284.